ORIGINAL RESEARCH

Construction of injectable, pH sensitive, antibacterial, mineralized amino acid yolk-shell microspheres for potential minimally invasive treatment of bone infection

Zhenhua Chen*
Mengen Zhao*
Jie Zhang
Kang Zhou
Xiuli Ren
Xifan Mei

Jinzhou Medical University, Jinzhou, 121001, People's Republic of China

*These authors contributed equally to this work

Introduction: Treatment of infection within bone is difficult, and conventional surgical treatment brings intense pain to the patients physically and mentally. There is an urgent need to develop injectable nano- and/or micro-medicine for minimally invasive treatment of osteomyelitis.

Methods: In this paper, amino acid (L-lysine [Lys]) was mineralized into yolk-shell structured $CaCO_3$ microspheres (MSs). The morphologies of the obtained MSs were investigated by scanning electron microscopy and transmission electron microscopy. The composition of $CaCO_3$ MSs was identified by using Fourier transform infrared spectroscopy. The as-prepared $CaCO_3$ MSs were examined with power X-ray diffraction analysis to obtain the crystallographic structure of the MSs.

Results: The as prepared Lys encapsulated $CaCO_3$ MSs (Lys@$CaCO_3$ MSs) were used as micro-drug to improve acidic environment of osteomyelitis caused by bacterial infection and promote osteoblast proliferation under oxidative stress. These pH responsive Lys@$CaCO_3$ MSs have a drug loading efficiency of 89.8 wt % and drug loading content (DLC) of 22.3 wt %.

Conclusion: Our results demonstrated that Lys@$CaCO_3$ MSs can effectively kill *Staphylococcus aureus* and promote proliferation and differentiation of osteoblasts under stimulation of H_2O_2 at pH = 5.5.

Keywords: osteomyelitis, oxidative stress, L-Lysine, micro-medicine, delivery vehicle

Introduction

Osteomyelitis is an inflammatory response of bone marrow, cortex, and periosteum caused by bacterial infection.[1,2] The current approach for treating osteomyelitis is mainly clinical surgery with the aid of high-dose antibiotics, which may cause antibiotic resistance and intense pain for the patients physically and mentally.[3–5] Therefore, there is an urgent need to develop injectable nano- and/or micro-medicine for minimally invasive treatment of osteomyelitis.

Previous studies have shown that oxidative stress plays an important role in regulating apoptosis of osteoblasts.[6,7] It is very important that injectable nano- and/or micro-medicine promotes osteoblast proliferation under oxidative stress in the osteomyelitis microenvironment. Recently, L-lysine (Lys) has attracted extensive attention because of reducing inflammatory response.[8,9] Currently, the development of nano- and/or micro-spheres to form nano- or micro-medicine to promote osteoblast proliferation has been documented.[10–12] This strategy permits loading large quantities of drugs and smart stimulus response release mechanism.[13–16] However, as far as amino acid

Correspondence: Zhenhua Chen; Xifan Mei
Jinzhou Medical University, Section 3, Number 40, Songpo Road, Jinzhou 121001, People's Republic of China
Email zhchen561@yahoo.com; meixifan1971@163.com

is concerned, it has seldom been reported as injectable, pH-responsive micro-medicine.

Herein, in this paper, we use a facile, one-pot method to construct injectable, pH sensitive, antibacterial, mineralized amino acid (Lys) yolk-shell structured microspheres (MSs) for potentially minimally invasive treatment of bone infection in situ. Hesperidin (Hesp), which has been reported to regulate the formation of $CaCO_3$ MSs in our former work,[17] was chosen as mineralization modifier. The protocol was altered from our previous work,[17] carbonate source changed from $(NH_4)_2CO_3$ to $NaHCO_3$. This change could provide an advantage when preparing yolk-shell structured products. The detailed steps are illustrated in Scheme 1. Firstly, our protocol included making an aqueous solution of Lys, Ca^{2+}, and Hesp. Thus, Ca^{2+} would be modified by the interactions with −OH (Hesp molecules) and nucleated into Ca-Hesp clusters. At the same time, Lys could be encapsulated into these clusters by the interaction between −NH_2 (Lys molecules) and Ca^{2+} or −OH from Hesp molecules, resulting in Ca-Hesp-Lys complexes. Subsequently, $NaHCO_3$ solution was added into the aqueous solution drop by drop. Thus, these HCO_3^- were attracted by Ca^{2+} from Ca-Hesp-Lys complexes, which provide sites for

further nucleation. Due to the instability of HCO_3^- at higher temperatures, the out layer of the HCO_3^--Ca-Hesp-Lys complexes will be converted into $CaCO_3$ (as the shell of $CaCO_3$ MSs). The inner part of the complexes will be transported into the core of $CaCO_3$ MSs with diffusion of NH_3 (which can react with HCO_3^- to form CO_3^{2-}). Finally, the yolk-shell structured Lys@$CaCO_3$ MSs were obtained after aging for a certain amount of time. Lys was encapsulated in the core, shell, and the void space. As illustrated in Scheme 2, Lys@$CaCO_3$ MSs can improve the acidic environment of osteomyelitis due to the dissolution or fracture of $CaCO_3$, while the released Lys can treat the damage caused by oxidative stress. Therefore, our strategy of mineralizing amino acid into yolk-shell MSs is facile, biocompatible, and pH sensitive MSs is highly promising for treating osteomyelitis.

Experiments
Materials
Hesp and Lys ($C_6H_{14}N_2O_2 \cdot HCl$) were purchased from Sigma-Aldrich Co. (St Louis, MO, USA). $CaCl_2$ (analytical reagent), $NaHCO_3$ (analytical reagent), and $NH_3 \cdot H_2O$ (analytical reagent) were purchased from Sinopharm Chemical Regent
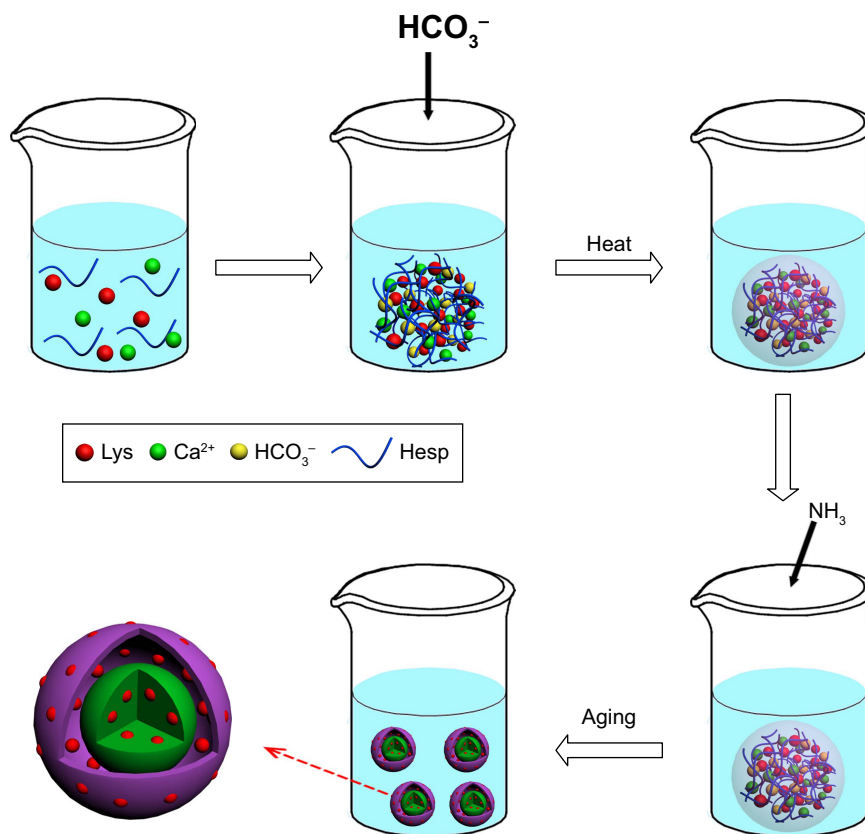
Scheme 1 The preparation process of the yolk-shell structured Lys@$CaCO_3$ MSs.
Note: $CaCO_3$ is indicated with purple for the shell and green for the core.
Abbreviations: Hesp, hesperidin; Lys, L-lysine; MSs, microspheres.
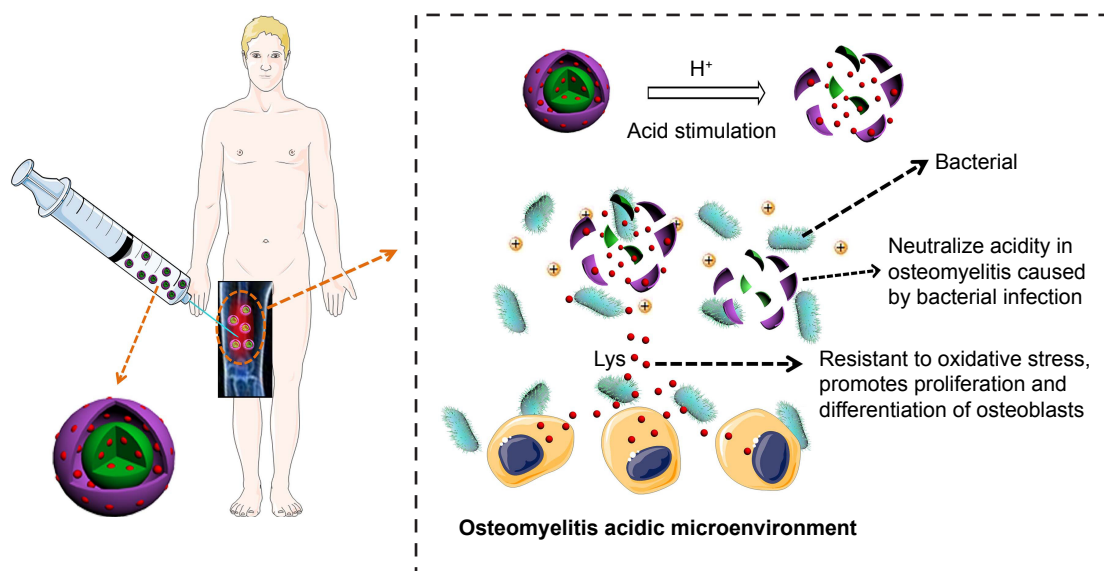
Scheme 2 Illustration of antibacterial, injectable, and pH sensitive Lys@CaCO₃ MSs used for potentially minimally invasive treatment of osteomyelitis.
Notes: CaCO₃ is indicated with purple for the shell and green for the core. Red indicates Lys.
Abbreviations: Lys, L-lysine; MSs, microspheres.

Co., Ltd. (Shanghai, People's Republic of China). Triply distilled deionized water was used during all the applications.

Preparation of the Lys@CaCO₃ MSs

The yolk-shell structured Lys@CaCO₃ MSs were synthesized with a facile, one-pot method. Firstly, 0.4% (wt %) Hesp solution was prepared by alkaline aqueous solution (pH = 11.0, adjusted with ammonia and HCl). Then, a solution of $CaCl_2$ (5 mL, 0.5 mol/L), as-prepared Hesp solution (5 mL), and Lys (60 mg) were added into a beaker (150 mL), where 80 mL water was further added. Subsequently, $NaHCO_3$ (10 mL, 1 mol/L) was added. The mixture was stirred using vortex mixing (IKA, Vortex, Genius 3) to obtain a homogeneous solution. After that, the solution was heated to 65°C and kept for 20 min. The beaker and 100 mL ammonia (in another beaker) were placed in a closed desiccator for 24 h at room temperature. By NH_3 (diffused from ammonia) dissolving in the solution, the mineralization of the yolk-shell structured Lys@CaCO₃ MSs was initiated. The products were collected by centrifugation and then rinsed with deionized water several times. Finally, the obtained products were dried at 70°C for further analysis.

Characterization

The morphologies of the obtained MSs were investigated by scanning electron microscopy (SEM; S4800, Hitachi Ltd., Tokyo, Japan) and transmission electron microscopy (TEM; JEM-1200EX; JEOL, Tokyo, Japan). The composition of CaCO₃ MSs was identified by using Fourier transform infrared spectroscopy (FTIR; Shimadzu, Kyoto, Japan) in the

range of 4,000 to 400 cm^{-1} with the KBr disk method. The as-prepared CaCO₃ MSs were examined with power X-ray diffraction (XRD) analysis (Shimadzu) with Cu Kα radiation to obtain the crystallographic structure of the MSs.

The thermogravimetric (TG) data of the samples were assessed with a Netzsch STA 449CDSC/DTA-TG analyzer (Netzsch-Gerätebau GmbH, Selb, Germany) scanning from 30 to 600°C under an air atmosphere. The samples were weighed and introduced into aluminum pans. The pans were heated at a constant rate of 10°C/min in an nitrogen atmosphere with an empty aluminum pan as the reference probe. The sample mass was in the range of 8–10 mg. All samples were run in duplicate.

Investigation of Lys release from Lys@CaCO₃ MSs

Acetate buffers (pH = 5.5) and PBS (pH = 7.4) were used for pH sensitivity investigation. Target samples were dispersed in the buffers and stirred for 5–10 minutes. The samples were centrifuged and the supernatant solutions were analyzed by an automatic potentiometric titrator (Excellence Titrator T9; Mettler-Toledo, LLC, Columbus, OH, USA). The release condition was set as 37°C, 1 atm pressure.

Cell and antibacterial experiment

Pre-osteoblasts (MC3T3E1) purchased from Type Culture Collection of the Chinese Academy of Sciences (Shanghai, People's Republic of China) were used as osteoblast cellular model. MTT assay was used to evaluate the proliferation or

apoptosis of osteoblasts in the different culture conditions. Firstly, osteoblasts were seeded at a density of 1,000 cells per well (96-well plate) and cultured for 24 h. Subsequently, the culture medium was removed and replaced by a series of Lys (0 mM, 0.2 mM, 0.4 mM, 0.6 mM, 0.8 mM) and Lys@CaCO$_3$ MSs (within 0 mM, 0.2 mM, 0.4 mM, 0.6 mM, 0.8 mM Lys) containing H$_2$O$_2$ (80 µM) at pH = 7.4 and 5.5 for 6 h. Then, 20 µL of MTT solution (5 mg/mL in PBS) was added into each well. After being treated for 4 h, the MTT medium was removed. Finally, 150 µL of DMSO was added into each well. Quantitative detection was performed on a microplate reader at the wavelength of 490 nm. To further investigate the resistance to oxidative stress of Lys@CaCO$_3$ MSs in acidic conditions, osteoblasts were seeded in a 12-well plate and treated with Krebs (control), H$_2$O$_2$ (80 µM), Lys (0.8 mM)+H$_2$O$_2$ (80 µM), and Lys@CaCO$_3$ MSs (within 0.8 mM Lys)+H$_2$O$_2$ (80 µM) at pH = 7.4 and 5.5 for 6 h.

Before confocal laser scanning microscopy (CLSM) images were taken, Lys@CaCO$_3$ MSs were stained green by FITC, cell nuclei were stained blue by Hoechst 33258, and the cytoskeleton was stained red by phalloidin. The detailed staining steps were in accordance with our previous work.[18–20]

Gram-positive *Staphylococcus aureus* (*S. aureus*, ATCC 35696) was chosen. *S. aureus* was cultured at 37°C in a liquid Luria-Bertani medium at 300 rpm in a rotary shaker with and without Lys@CaCO$_3$ MSs for a certain amount of time. Then, the turbidity at 600 nm was measured by a Hitachi U-3010 spectrophotometer.

Western blot analysis and PCR

In each group, after being incubated for a certain amount of time, osteoblast cells were lysed immediately in Laemmli buffer. Equal amounts of protein from each group were prepared using bicinchoninic acid and separated by sodium dodecyl sulfate/polyacrylamide gel electrophoresis. The proteins were transferred electrophoretically from the gels to PVDF membranes, which were then treated with anti-mouse Wnt3a and β-catenin antibodies overnight at 4°C. Subsequently, they were treated with a corresponding secondary antibody for 1 h. Immunoreactive proteins were revealed by using an enhanced chemiluminescence kit (Pierce Chemical, Rockford, IL, USA). Expression of GAPDH was used as the control. The autoradiograms were carried out on an Alpha Innotech Photo documentation System (Alpha Innotech, Hayward, CA, USA). The relative absorbance of the bands, representing the amount of protein expression, was analyzed using Quantity One software (Bio-Rad Laboratories Inc., Hercules, CA, USA).

After being incubated for a certain amount of time, the culture medium was used to determine the Wnt3a and β-catenin protein content using PCR, according to literature.[21]

Results and discussion

SEM image (Figure 1A) clearly shows the morphology of the obtained CaCO$_3$ crystals – MSs (2–5 µm in diameter). Figure 1B reveals the detailed morphology of a single Lys@CaCO$_3$ MS having a rough surface. It is clear that the porous surface of such MS is composed of units of numerous small particles. TEM image in Figure 1C shows the yolk-shell structure of the obtained products with a thin shell and a condensed core. The magnified TEM image (Figure 1D) shows the detailed structure of the shell. It is the aggregate of many spherical nanocrystals with an average size of approximately 30 nm in diameter.

Figure 2 presents the FTIR spectra of CaCO$_3$ MSs without Lys, Lys and Lys@CaCO$_3$ MSs. Figure 2A shows CaCO$_3$ MSs with the characteristic absorption peaks of calcite located at 710 and 876 cm^{-1} and vaterite at 746 cm^{-1}. This suggests that the prepared CaCO$_3$ MSs have a mixed crystalline phase of calcite and vaterite.[17] It also indicates that the characteristic peak intensity of calcite is stronger than that of vaterite, which may suggest that calcite is the dominating crystalline phase. For Lys@CaCO$_3$ MSs, the broad absorption peak ranging from 896 to 823 cm^{-1} may be ascribed to the combined peaks from Lys and CaCO$_3$. These data indicate that the obtained CaCO$_3$ MSs have been incorporated with Lys.

The XRD pattern result shown in Figure 3 further proved the polycrystalline property of the Lys@CaCO$_3$ MSs. The reflections at 2θ = 21.1, 29.6, 36.0, 39.5, 47.2, 47.8, 48.6, and 65.2° are attributable to reflecting planes of calcite (Joint Committee on Powder Diffraction Standards [JCPDS], card no 83-0578), while reflections at 23.1, 25.1, 27.3, 32.9, 43.9, 50.3 and 55.8° are assigned to the reflecting planes of vaterite (JCPDS, card no 72-0506). Rao's equation was adopted to calculate the relative fraction of vaterite (f_V) and calcite (f_C) in crystalline phase according to the literature:[22,23]

$$f_V = \frac{I_{110V} + I_{112V} + I_{114V}}{I_{110V} + I_{112V} + I_{114V} + I_{104C}} \tag{1}$$

The result indicates that calcite and vaterite contents in yolk-shell structured CaCO$_3$ MSs are 79.99% and 20.01%, respectively.

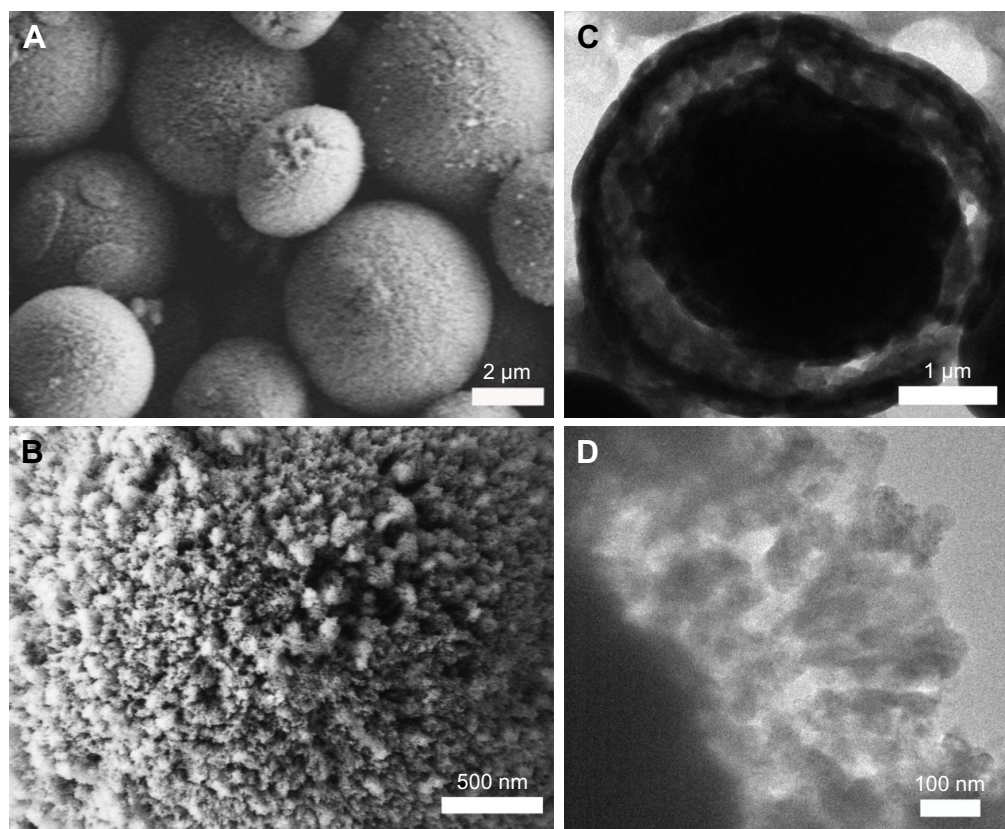Potentiometric titration (Figure 4A–C) was used to measure the concentration of the Lys released from the

Figure 1 SEM and TEM images.
Notes: (**A**) SEM image of yolk-shell structured Lys@CaCO$_3$ MSs obtained. (**B**) Surface magnified SEM image of the obtained Lys@CaCO$_3$ MSs. (**C**) TEM image of the obtained Lys@CaCO$_3$ MSs; (**D**) high-resolution inset of TEM image of the edge of the microsphere.
Abbreviations: Lys, L-lysine; MSs, microspheres; SEM, scanning electron microscopy; TEM, transmission electron microscopy.
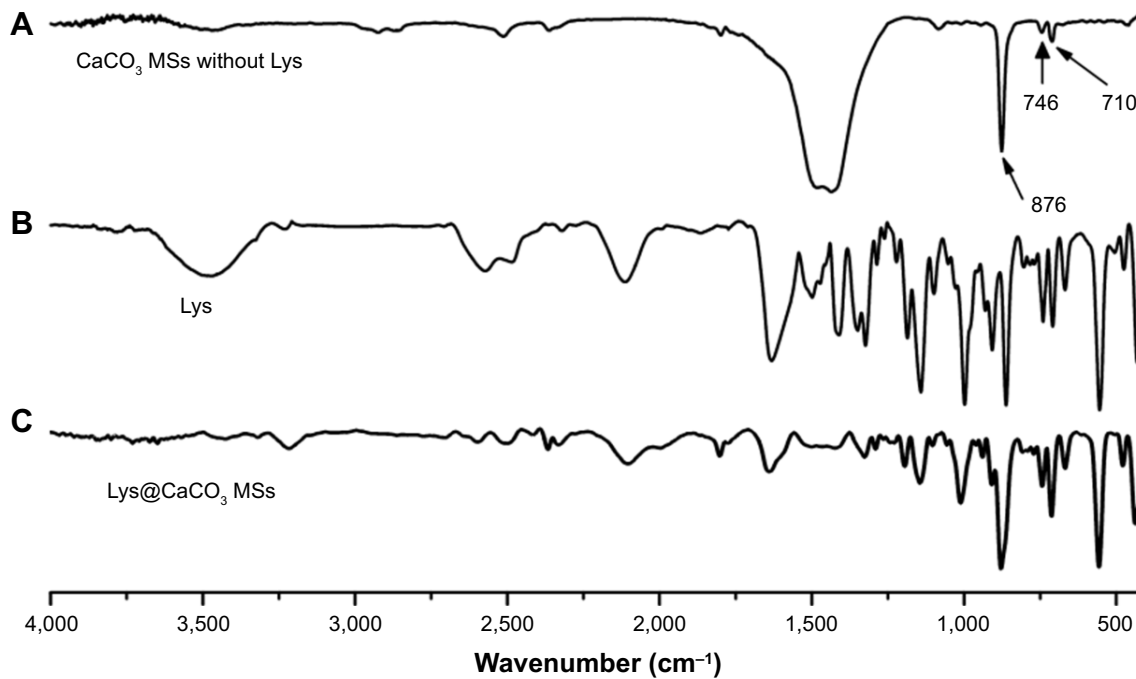

Figure 2 FTIR spectra of the samples.
Notes: (**A**) CaCO$_3$ MSs without Lys; (**B**) Lys; (**C**) Lys@CaCO$_3$ MSs. The arrows indicate the absorption peaks of calcite located at 710 and 876 cm^{-1}; and vaterite at 746 cm^{-1}.
Abbreviations: FTIR, Fourier transform infrared spectroscopy; Lys, L-lysine; MSs, microspheres.
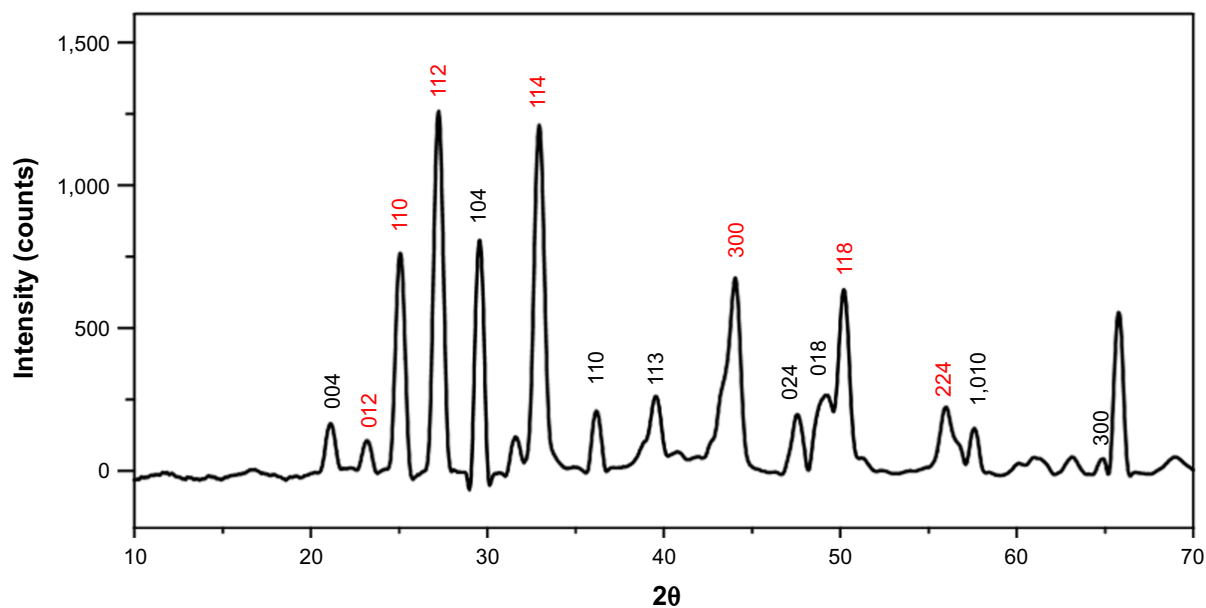
Figure 3 XRD reflections.
Note: XRD reflection indicates Lys@CaCO$_3$ microspheres bearing reflection of standard calcite (black) and vaterite (red), respectively.
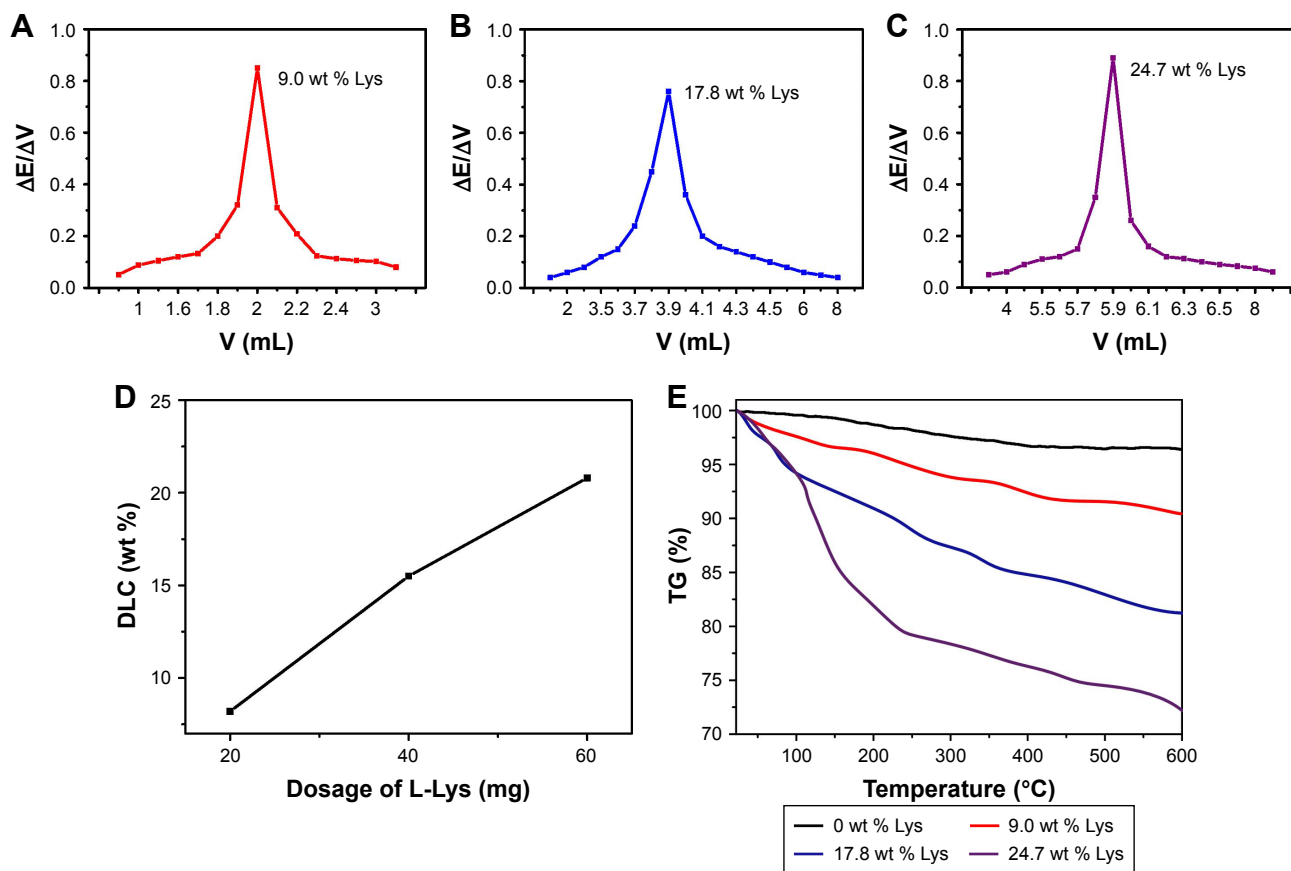**Abbreviations:** Lys, L-lysine; XRD, X-ray diffraction.

Figure 4 Potentiometric titration results and TG analysis.
Notes: Potentiometric titration curve of the different amounts of Lys within the obtained Lys@CaCO$_3$ MSs. (**A**) 9.0 wt %, (**B**) 17.8 wt %, (**C**) 24.7 wt %; (**D**) initial amounts of Lys during the synthesis of Lys@CaCO$_3$ MSs versus the DLC; (**E**) TG curves of the obtained Lys@CaCO$_3$ MSs.
Abbreviations: DLC, drug loading content; E, potentio; Lys, L-lysine; MSs, microspheres; TG, thermogravimetric; V, volume.

obtained Lys@CaCO$_3$ MSs. Perchloric acid titration solution (0.1 mol/L) of 2.0 mL, 3.9 mL, and 5.9 mL was consumed by Lys within the obtained Lys@CaCO$_3$ MSs when the different amounts of Lys (9 wt %, 17.8 wt %, 24.7 wt %) were added in the preparation of Lys@CaCO$_3$ MSs. The corresponding drug loading content (DLC) of Lys (8.2%, 15.8%, and 22.3%, shown in Figure 4D) was calculated by the following equation:

$$DLC = \frac{m}{M} \times 100\% \qquad (2)$$

where m is the mass of Lys determined by potentiometric titration; M is the mass of CaCO$_3$ MSs used to load Lys in each group.

Figure 4A–D revealed that the maximum DLC of the Lys@CaCO$_3$ MSs was 22.3 wt % when the 24.7 wt % Lys was added. Moreover, the drug loading efficiency (DLE) of the Lys@CaCO$_3$ MSs was 89.8%. TG curves of the as-synthesized samples are shown in Figure 4E. After increasing the temperature, there was no significant weight loss for CaCO$_3$ MSs without Lys. However, a significant weight loss

was observed for the obtained Lys@CaCO$_3$ MSs (the different amounts of Lys encapsulated), due to the combustion of Lys. TG analysis was consistent with previous experimental results (Figure 4D). It was found that the loading of Lys on Lys@CaCO$_3$ MSs increased with the increase of Lys dosage. The maximum DLC of the Lys@CaCO$_3$ MSs was studied based on the previously mentioned experimental results.

Figure 5 presents the CLSM images of osteoblasts cultured under different conditions, which reveal the morphology change of osteoblasts. Figure 5A presents the image of normal osteoblasts cultured at pH = 7.4, which are full in shape (indicated by arrows) at the stage of normal proliferation and differentiation. However, Figure 5B shows the osteoblasts (indicated by arrows) which became flat or shorter at pH = 5.5 (simulating the mildly acidic microenvironment of osteomyelitis). This might be because the acidic environment is detrimental to the growth of osteoblasts. Osteoblasts became shorter or even died (indicated by arrows, Figure 5C) when cultured under H$_2$O$_2$ (80 µM, simulating oxidative stress conditions) at pH = 5.5. Figure 5D shows the osteoblasts which became relatively longer in the presence of Lys (0.8 mM) due to the anti-oxidation property of
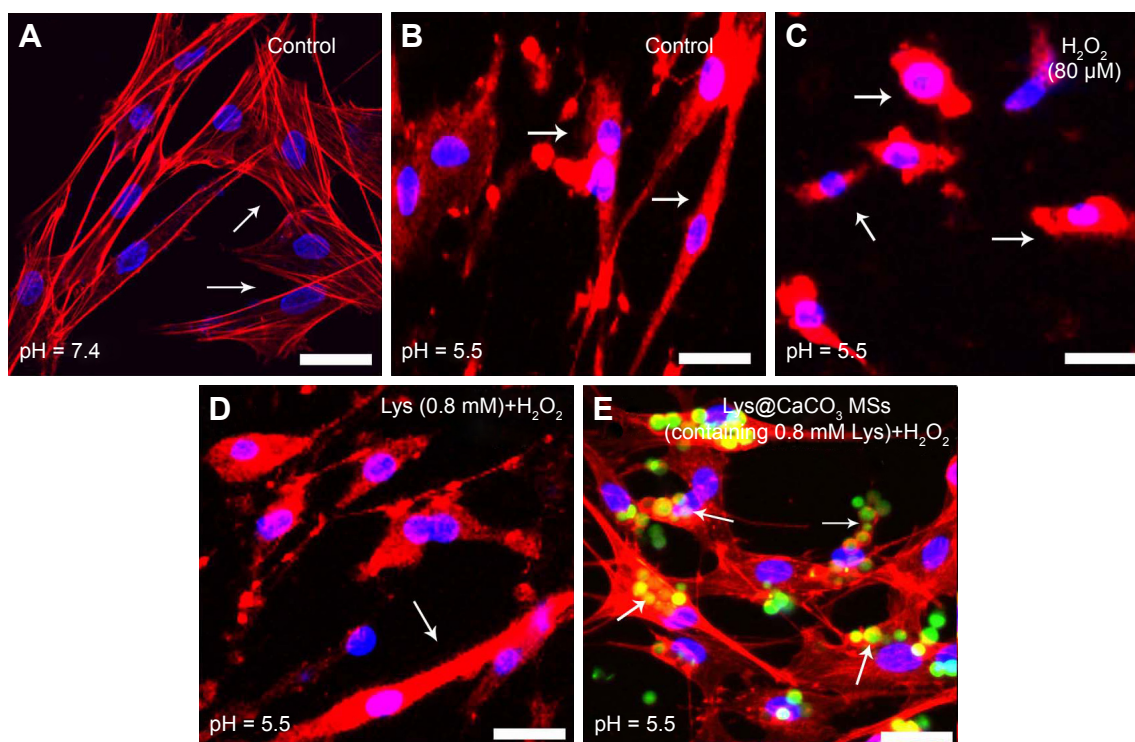

Figure 5 Confocal laser scanning microscopy (CLSM) images of shape of osteoblasts cultured under different conditions.
Notes: (**A**) At pH = 7.4, without H$_2$O$_2$; (**B**) at pH = 5.5, without H$_2$O$_2$; (**C**) at pH = 5.5, 80 µM H$_2$O$_2$; (**D**) at pH = 5.5, 80 µM H$_2$O$_2$, 0.8 µM Lys; (**E**) at pH = 5.5, 80 µM H$_2$O$_2$, Lys@CaCO$_3$ MSs (containing 0.8 µM Lys). The scale bars are 30 µm. Arrows in **A–D** indicate the classical cells under each condition. Arrows in **E** indicate the CaCO$_3$ MSs.
Abbreviations: Lys, L-lysine; MSs, microspheres.

Lys. However, the osteoblasts were still flat, because the acidic environment still made osteoblasts grow abnormally. Osteoblasts' morphology returned to normal, full in shape (Figure 5E) by adding Lys@CaCO$_3$ MSs (containing 0.8 mM Lys). The possible reason being, when Lys was released from Lys@CaCO$_3$ MSs, the acidic environment was neutralized by the dissolution of CaCO$_3$. Figure 5E also shows that some Lys@CaCO$_3$ MSs (stained green, indicated by arrows) were not completely dissolved.

From these changes in morphology results, it can be inferred that Lys@CaCO$_3$ MSs can help osteoblasts to resist acidic pH and H$_2$O$_2$. Figure 6 further indicates the effect of Lys@CaCO$_3$ MSs on the proliferation and differentiation of osteoblasts. Figure 6E–H shows the significant inhibition of osteoblasts by H$_2$O$_2$ (80 μM) compared with the control group (Figure 6A–D). It is obvious that this was slightly improved in the Lys+H$_2$O$_2$-treated group (Figure 6I–L). The osteoblasts returned to normal in the Lys@CaCO$_3$

MSs+H$_2$O$_2$-treated group (Figure 6M–P). Figure 6O and P show that a small amount of Lys@CaCO$_3$ MSs (labeled by FITC, indicated by arrows) was not dissolved.

The release of Lys from Lys@CaCO$_3$ MSs (Figure 7A), took place at different pH conditions (pH = 5.5 and pH = 7.4). The release amount was only 11.2% in PBS buffer (pH = 7.4) after dialysis for 6 h. When the release time increased from 6 h to 8 h, the release amount of Lys did not obviously increase. This indicated that most of the Lys was still stored in the Lys@CaCO$_3$ MSs, the measured small amount of Lys might be due to the surface-adsorbed ones. At pH = 5.5, 39.8% Lys was released within 1 h, and approximately 100% was released at about 8 h. These results demonstrate that the release of Lys from Lys@CaCO$_3$ MSs was strongly pH-dependent.

MTT method was used to further investigate the effect of Lys@CaCO$_3$ MSs on cell viability of osteoblasts at different pH conditions. Figure 7B shows the compared cell viability
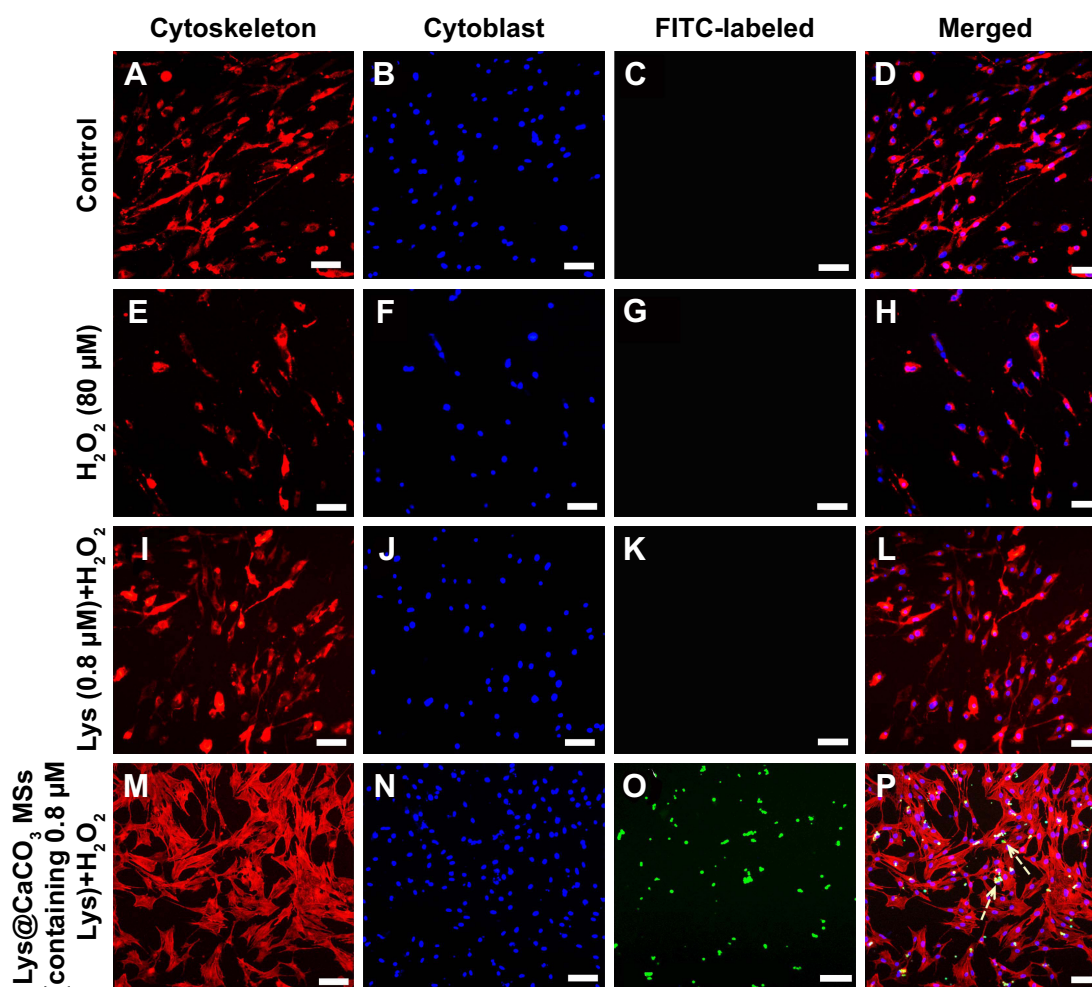

Figure 6 Confocal laser scanning microscopy (CLSM) images show the cell density of osteoblasts cultured under different conditions.
Notes: At pH = 5.5: (**A–D**) control group, without H$_2$O$_2$; (**E–H**) with 80 μM H$_2$O$_2$; (**I–L**) with 80 μM H$_2$O$_2$, 0.8 μM Lys; and (**M–P**) with 80 μM H$_2$O$_2$, Lys@CaCO$_3$ MSs (containing 0.8 μM Lys). The scale bars are 100 μm.
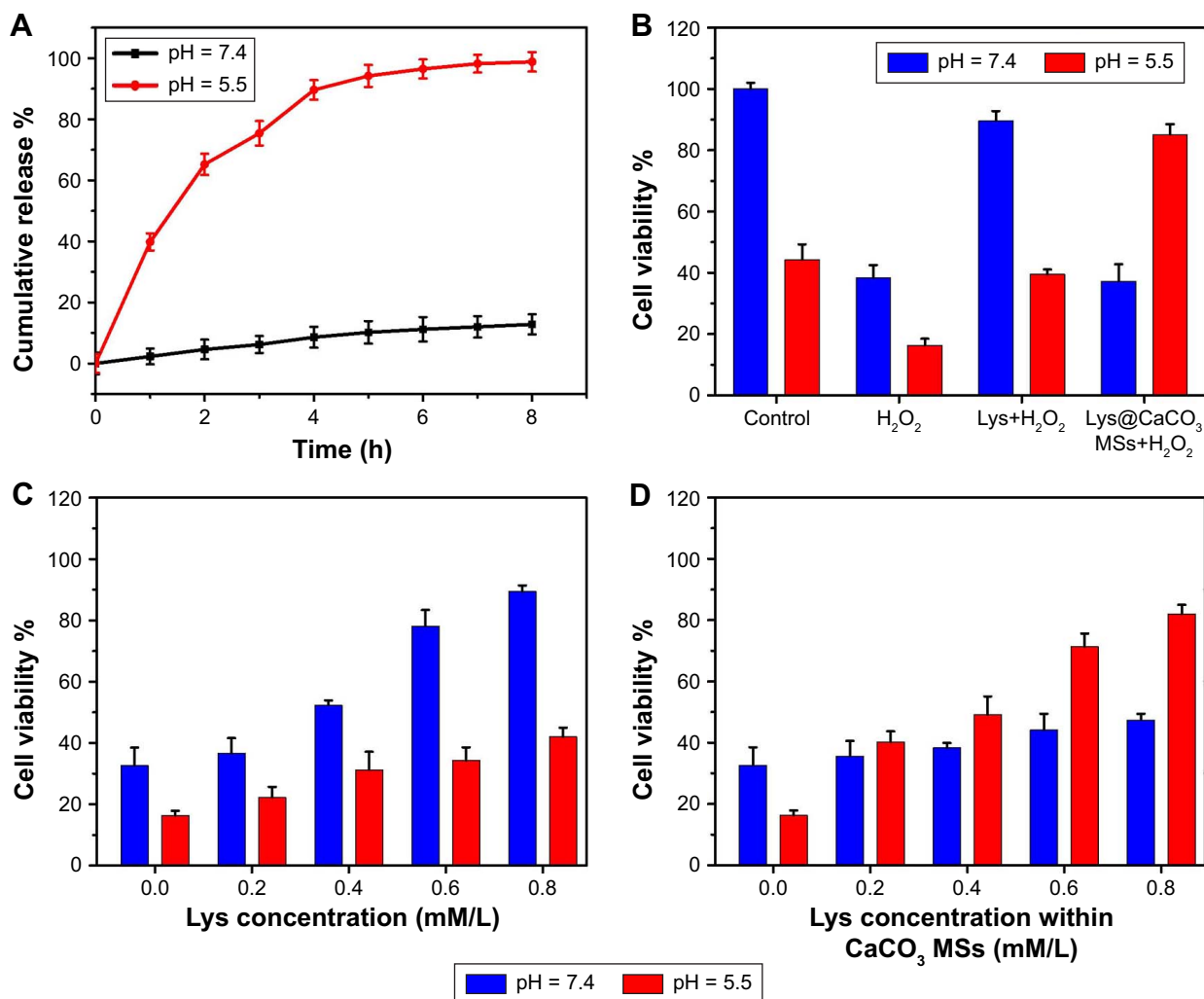**Abbreviations:** Lys, L-lysine; MSs, microspheres.

Figure 7 Lys release results and cell viability studies of osteoblasts.
Notes: (**A**) The release profiles of Lys from Lys@CaCO$_3$ MSs at pH = 7.4 and 5.5. (**B**) Cell viability studies of osteoblasts cultured under different conditions. Cell viability studies of osteoblasts faced with free Lys (**C**) and Lys@CaCO$_3$ MSs (**D**) with varying concentrations of Lys at pH = 7.4 and 5.5 treated with H$_2$O$_2$.
Abbreviations: Lys, L-lysine; MSs, microspheres.

results of osteoblasts in control, H$_2$O$_2$ (80 μM)-treated, Lys (0.8 mM)+H$_2$O$_2$ (80 μM)-treated, and Lys@CaCO$_3$ MSs (within 0.8 mM Lys)+H$_2$O$_2$ (80 μM)-treated groups at different pH values. The results reveal that cell viability decreased due to the stimulation of H$_2$O$_2$ and acid. At pH = 7.4, free Lys could significantly increase cell viability by resisting H$_2$O$_2$. However, at pH = 5.5, Lys could not increase cell viability as at pH = 7.4. However, Lys@CaCO$_3$ MSs could significantly increase cell viability in the presence of H$_2$O$_2$ at pH = 5.5. Figure 7C indicates that cell viability was obviously increased by increasing Lys concentration at pH = 7.4. However, when pH was changed from 7.4 to 5.5, cell viability increased slowly due to increasing Lys concentration. On the other hand, at pH = 7.4, increasing Lys@CaCO$_3$ MSs' concentration did not cause a significant difference in cell viability (Figure 7D). At pH = 5.5, the cell viability quickly increased up to 83.6% by increasing the concentration to

0.8 mM Lys (within Lys@CaCO$_3$ MSs). These results reveal an evidently acidity-enhanced release of Lys (to resist H$_2$O$_2$) which increased cell proliferation because of the degradation of CaCO$_3$.

To further consolidate our inference, we also evaluated cell viability of osteoblasts in the presence of free Lys and Lys@CaCO$_3$ MSs versus different culture times under the stimulation of H$_2$O$_2$ (80 μM) at pH = 5.5. The results were shown in Figure 8. There was a slightly decreased cell viability both in Lys-treated group and Lys@CaCO$_3$ MSs-treated group in the first 2 h. As acid has a strong lethality to cells, cell activity of osteoblasts continued to decline after 2 h in the pure Lys-treated group. For the Lys@ CaCO$_3$ MSs group, after 2 h, cell activity became increased because of the continuous release of Lys (to resist H$_2$O$_2$) by degradation of CaCO$_3$ MSs. At the same time, this degradation neutralized the acidic microenvironment, which was
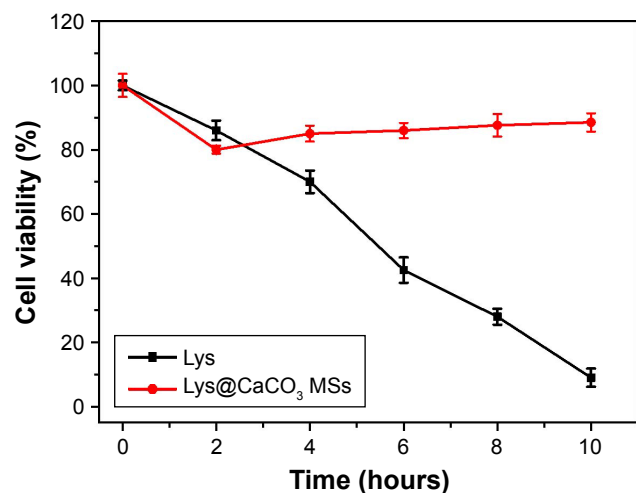
Figure 8 The change in cell viability of osteoblasts according to culture time in Lys (0.8 mM)-treated and Lys@CaCO$_3$ MSs (containing 0.8 mM Lys)-treated groups under stimulation of H$_2$O$_2$ (80 µM) at pH = 5.5.
Abbreviations: Lys, L-lysine; MSs, microspheres.

beneficial for the growth of osteoblasts. The antibacterial property of Lys@CaCO$_3$ MSs is shown in Figure S1, in the control group, there was an obvious increase of turbidity, indicative of *S. aureus* growth, while, compared to the control group, the turbidity decreased when introducing Lys@CaCO$_3$ MSs into the culture system. From the inset image in Figure S1, it is obvious that there was much more *S. aureus* in the control group than in the group cultured with Lys@CaCO$_3$ MSs. This is probably due to the acidic microenvironment, caused by bacteria, being neutralized by CaCO$_3$, and a mild alkaline environment (produced by the dissolved mineral from Lys@CaCO$_3$ MSs) is not conducive to bacterial

growth.[18] The results in Figure S2 further indicate that Lys@CaCO$_3$ has antibiotic activity to *Escherichia coli* (a classic Gram-negative bacteria), similar to that of *S. aureus*. These data further confirm that Lys@CaCO$_3$ MSs have a promising antibacterial function.

It is known that the Wnt/β-catenin pathway plays an important role in the differentiation and proliferation of osteoblasts under inflammatory conditions.[24,25] Wnt proteins, such as Wnt1, Wnt2, Wnt3, Wnt3a, Wnt8, and Wnt8b, are significant as the starting factor for the Wnt/β-catenin pathway.[26] Moreover, β-catenin is a hub-type signaling molecule in the Wnt/β-catenin pathway, and its expression level is one of the common indicators for detecting the activation level of Wnt/β-catenin pathway.[27] Herein, we collected the gene expression of Wnt3a and β-catenin to explain the possible mechanism. Semi-quantitative RT-PCR data (Figure 9) show that the expression of Wnt3a and β-catenin increased after Lys+H$_2$O$_2$ treatment compared with H$_2$O$_2$ treatment in an acidic environment. Due to the acidic environment being neutralized by dissolution of CaCO$_3$ MSs, with increased cell viability, the expression of Wnt3a and β-catenin increased significantly in the Lys@CaCO$_3$ MSs-treated group. In addition, Western blot assay (Figure 10A) and quantification analysis results (Figure 10B and C) revealed that the expression of Wnt3a and β-catenin increased in Lys+H$_2$O$_2$-treated and Lys@CaCO$_3$ MSs+H$_2$O$_2$-treated groups compared to H$_2$O$_2$-treated group. Moreover, the upregulated expression of Wnt3a and β-catenin in the Lys@CaCO$_3$ MSs group was more obvious. Therefore, we believe that Lys@CaCO$_3$ MSs may regulate the Wnt3a and β-catenin factors in the classic
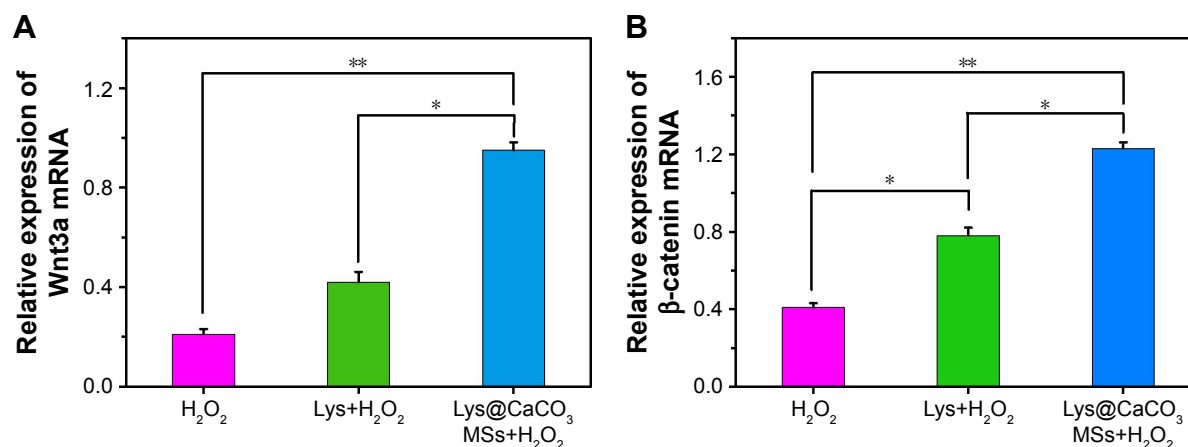

Figure 9 PCR analysis results.
Notes: Semi-quantitative expression of different genes in H$_2$O$_2$-treated, Lys (0.8 mM)+H$_2$O$_2$-treated and Lys@CaCO$_3$ MSs (containing 0.8 mM Lys)+H$_2$O$_2$-treated groups, respectively. (**A**) Wnt3a, (**B**) β-catenin (*$P<0.05$, **$P<0.01$, n = 3, each group treated with 80 µM H$_2$O$_2$ at pH = 5.5).
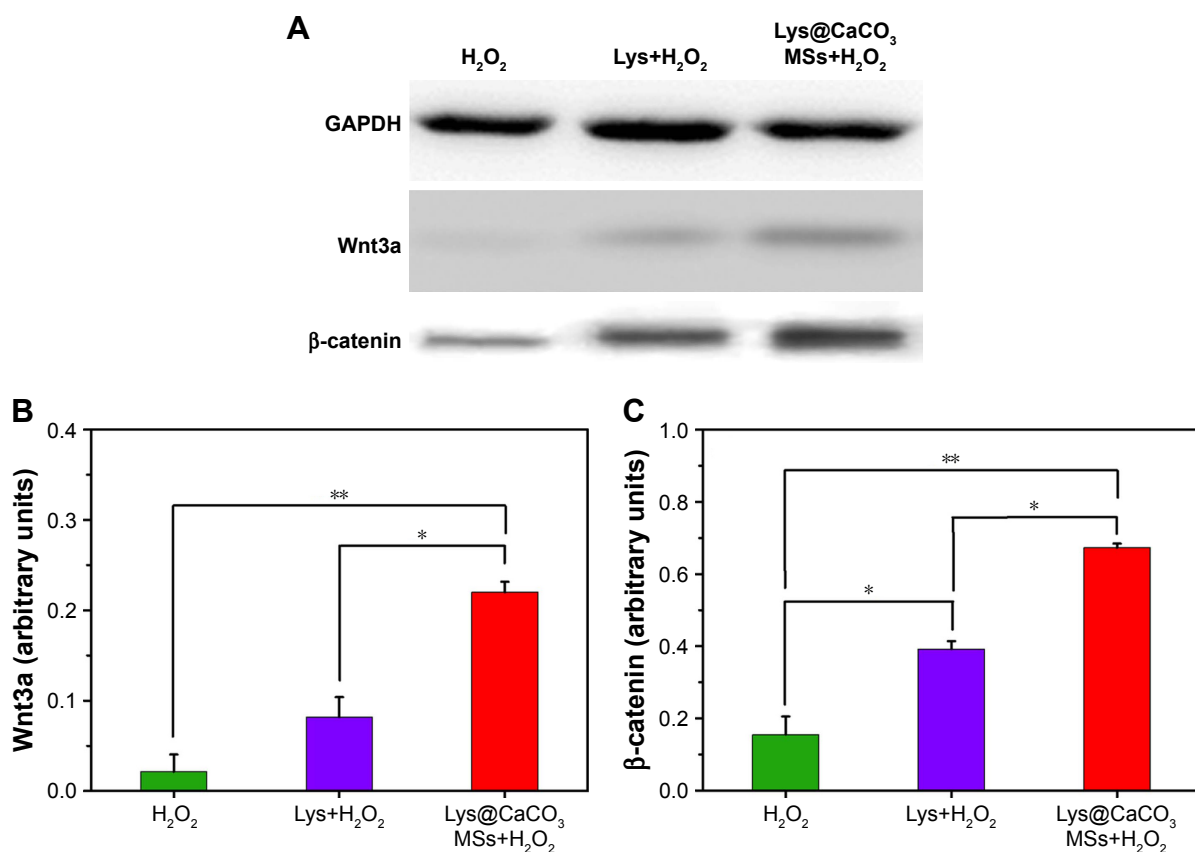**Abbreviations:** Lys, L-lysine; MSs, microspheres.

Figure 10 Western blot assay and quantification analysis.
Notes: (**A**) Western blot assay and quantification analysis results of the expression of Wnt3a (**B**) and β-catenin (**C**) in H_2O_2-treated, Lys (0.8 mM)+H_2O_2-treated and Lys@CaCO$_3$ MSs (containing 0.8 mM Lys)+H_2O_2-treated groups, respectively (*$P<0.05$, **$P<0.01$, n = 3, each group treated with 80 μM H_2O_2 at pH = 5.5). GAPDH used as control.
Abbreviations: Lys, L-lysine; MSs, microspheres.

Wnt/β-catenin pathway to promote the differentiation and proliferation of osteoblasts. At the same time, as the results in Figures S3 and S4 showed, Lys@CaCO$_3$ MSs can also increase the expression of OCN, OPN, and the activity of ALP after Lys+H_2O_2 treatment compared with H_2O_2 treatment in an acidic environment. Lys@CaCO$_3$ MSs reversed the oxidant-induced alterations in osteoblasts and may be a good option for treating osteomyelitis.

To develop micro-medicine for the treatment of osteomyelitis, there is still a long way to go. In addition to the data provided, we also give a future research plan here. We speculate that the addition of lysine can inhibit the differentiation of pre-osteoclasts into osteoclasts, but, unfortunately, it is difficult for us to obtain pre-osteoclasts in vitro. Therefore, this cannot be confirmed at present. Besides the limitation of osteoclasts, injectable properties of Lys@CaCO$_3$ MSs need to be confirmed by using an osteomyelitis animal model. The metabolism of MSs in vivo, including plasma concentrations, bone mass change, and blood calcium levels should be further investigated in the future. Further investigations about the

expression of inflammatory factors and osteogenic related proteins and genes in vivo also need to be carried out.

Conclusion

In this work, we reported the preparation of Lys@CaCO$_3$ MSs by a facile bio-inspired mineralization method at room temperature. The obtained Lys@CaCO$_3$ MSs had a DLE of 89.8 wt % and DLC of 22.3 wt %. The CLSM images indicated that Lys@CaCO$_3$ MSs can reverse the oxidant-induced alterations in osteoblasts. Besides, because of their excellent pH-responsive drug release, and the dissolution or fracture by itself for improving the local acidic environment of osteomyelitis, our results demonstrate that the obtained Lys@CaCO$_3$ MSs can efficiently promote proliferation and differentiation of osteoblasts, and may be a good option for treating osteomyelitis.

Acknowledgments

Disclosure

The authors report no conflicts of interest in this work.

References

1. Wu T, Zhang Q, Ren W, et al. Controlled release of gentamicin from gelatin/genipin reinforced beta-tricalcium phosphate scaffold for the treatment of osteomyelitis. *J Mater Chem B*. 2013;1(26):3304–3313.
2. Uskoković V, Batarni SS, Schweicher J, King A, Desai TA. The effect of calcium phosphate particle shape and size on their antibacterial and osteogenic activity in the delivery of antibiotics in vitro. *ACS Appl Mater Interfaces*. 2013;5(7):2422–2431.
3. Sedghizadeh PP, Sun S, Junka AF, et al. Design, synthesis, and antimicrobial evaluation of a novel bone-targeting bisphosphonate-ciprofloxacin conjugate for the treatment of osteomyelitis biofilms. *J Med Chem*. 2017;60(6):2326–2343.
4. Ghosh S, Wu V, Pernal S, Uskoković V. Self-setting calcium phosphate cements with tunable antibiotic release rates for advanced antimicrobial applications. *ACS Appl Mater Inter*. 2016;8(12):7691–7708.
5. Houghton TJ, Tanaka KS, Kang T, et al. Linking bisphosphonates to the free amino groups in fluoroquinolones: preparation of osteotropic prodrugs for the prevention of osteomyelitis. *J Med Chem*. 2008;51(21):6955–6969.
6. Golizeh M, Abusarah J, Benderdour M, Sleno L. Covalent binding of 4-hydroxynonenal to matrix metalloproteinase 13 studied by liquid chromatography-mass spectrometry. *Chem Res Toxicol*. 2014;27(9):1556–1565.
7. Chen Q, Shao X, Ling P, et al. Low molecular weight xanthan gum suppresses oxidative stress-induced apoptosis in rabbit chondrocytes. *Carbohyd Polym*. 2017;169:255–263.
8. Sahu K, Sharma M, Bansal H, Dube A, Gupta PK. Topical photodynamic treatment with poly-L-lysine-chlorin p6 conjugate improves wound healing by reducing hyperinflammatory response in Pseudomonas aeruginosa-infected wounds of mice. *Laser Med Sci*. 2013;28(2):465–471.
9. Singh BB, Udani J, Vinjamury SP, et al. Safety and effectiveness of an L-lysine, zinc, and herbal-based product on the treatment of facial and circumoral herpes. *Altern Med Rev*. 2005;10(2):123–127.
10. He W, Mosselhy DA, Zheng Y, et al. Effects of silica-gentamicin nanohybrids on osteogenic differentiation of human osteoblast-like SaOS-2 cells. *Int J Nanomedicine*. 2018;13:877–893.
11. Zhou J, Zhang Y, Li L, et al. Human β-defensin 3-combined gold nanoparticles for enhancement of osteogenic differentiation of human periodontal ligament cells in inflammatory microenvironments. *Int J Nanomedicine*. 2018;13:555–567.
12. Wang X, Zhang G, Qi F, et al. Enhanced bone regeneration using an insulin-loaded nano-hydroxyapatite/collagen/PLGA composite scaffold. *Int J Nanomedicine*. 2018;13:117–127.
13. Steinhilber D, Witting M, Zhang X, et al. Surfactant free preparation of biodegradable dendritic polyglycerol nanogels by inverse nanoprecipitation for encapsulation and release of pharmaceutical biomacromolecules. *J Control Release*. 2013;169(3):289–295.
14. Wu Z, Li Q, Pan Y, et al. Nanoporosity improved water absorption, in vitro degradability, mineralization, osteoblast responses and drug release of poly(butylene succinate)-based composite scaffolds containing nanoporous magnesium silicate compared with magnesium silicate. *Int J Nanomedicine*. 2017;12:3637–3651.
15. Parakhonskiy BV, Foss C, Carletti E, et al. Tailored intracellular delivery via a crystal phase transition in 400 nm vaterite particles. *Biomaterials Science*. 2013;12:1273–1281.
16. Wang Q, Huang JY, Li HQ, et al. Recent advances on smart TiO2 nanotube platforms for sustainable drug delivery applications. *Int J Nanomedicine*. 2017;12:151–165.
17. Yang T, Wan Z, Liu Z, et al. In situ mineralization of anticancer drug into calcium carbonate monodisperse nanospheres and their pH-responsive release property. *Mater Sci Eng C Mater Biol Appl*. 2016;63:384–392.
18. Zhang J, Zhao M, Tian X, et al. Protein-mediated mineralization of edaravone into injectable, pH-sensitive microspheres used for potential minimally invasive treatment of osteomyelitis. *New J Chem*. 2018;42(7):5447–5455.
19. Tian X, Zhang H, Zhang F, et al. Preparation of anticancer micromedicine based on quinoline and chitosan with pH responsive release performance. *Colloids Surf B Biointerfaces*. 2018;165:278–285.
20. Zhou K, Ren X, Zhao M, et al. Promoting proliferation and differentiation of BMSCs by green tea polyphenols functionalized porous calcium phosphate. *Regen Biomater*. 2018;5(1):35–41.
21. Liu Z, Shi W, Ji X, et al. Molecules mimicking Smad1 interacting with Hox stimulate bone formation. *J Biol Chem*. 2004;279(12):11313–11319.
22. Rao MS. Kinetics and mechanism of the transformation of vaterite to calcite. *Bull Chem Soc Jpn*. 1973;46(5):1414–1417.
23. Wang A, Yang Y, Zhang X, et al. Gelatin-Assisted Synthesis of Vaterite Nanoparticles with Higher Surface Area and Porosity as Anticancer Drug Containers In Vitro. *Chem Plus Chem*. 2016;81(2):194–201.
24. Nagano A, Arioka M, Takahashi-Yanaga F, Matsuzaki E, Sasaguri T. Celecoxib inhibits osteoblast maturation by suppressing the expression of Wnt target genes. *J Pharmacol Sci*. 2017;133(1):18–24.
25. Liu W, Konermann A, Guo T, et al. Canonical Wnt signaling differently modulates osteogenic differentiation of mesenchymal stem cells derived from bone marrow and from periodontal ligament under inflammatory condition. *BBA-Gen Subjects*. 2014;1840(3):1125–1134.
26. Lako M, Lindsay S, Lincoln J, et al. Characterisation of Wnt gene expression during the differentiation of murine embryonic stem cells in vitro: role of Wnt3 in enhancing haematopoietic differentiation. *Mech Develop*. 2001;103(1–2):49–59.
27. Valkenburg KC, Graveel CR, Zylstra-Diegel CR, Zhong Z, Williams BO. Wnt/β-catenin signaling in normal and cancer stem cells. *Cancers (Basel)*. 2011;3(2):2050–2079.
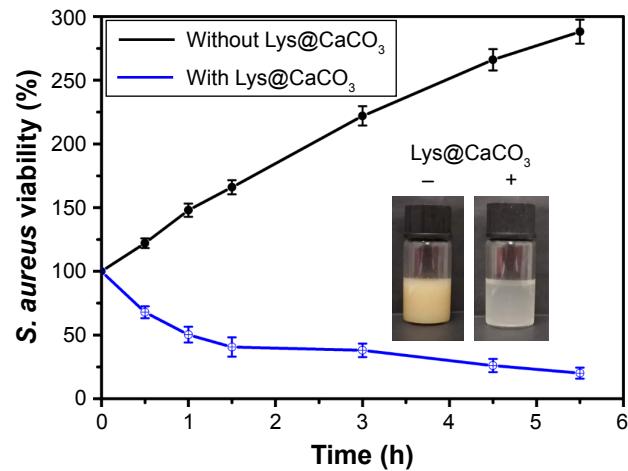
Supplementary materials

Figure S1 Time-dependent viability of *Staphylococcus aureus* (calculated by turbidity at 600 nm) co-cultured with and without Lys@CaCO$_3$.
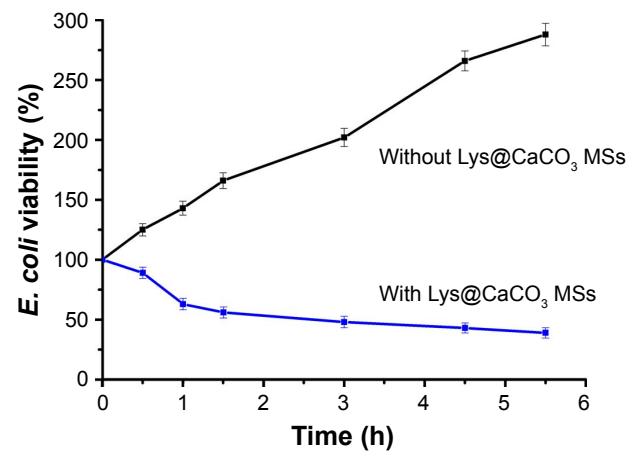**Abbreviation:** Lys, L-lysine.

Figure S2 Time-dependent viability of *Escherichia coli* (calculated by turbidity at 600 nm) co-cultured with and without Lys@CaCO$_3$.
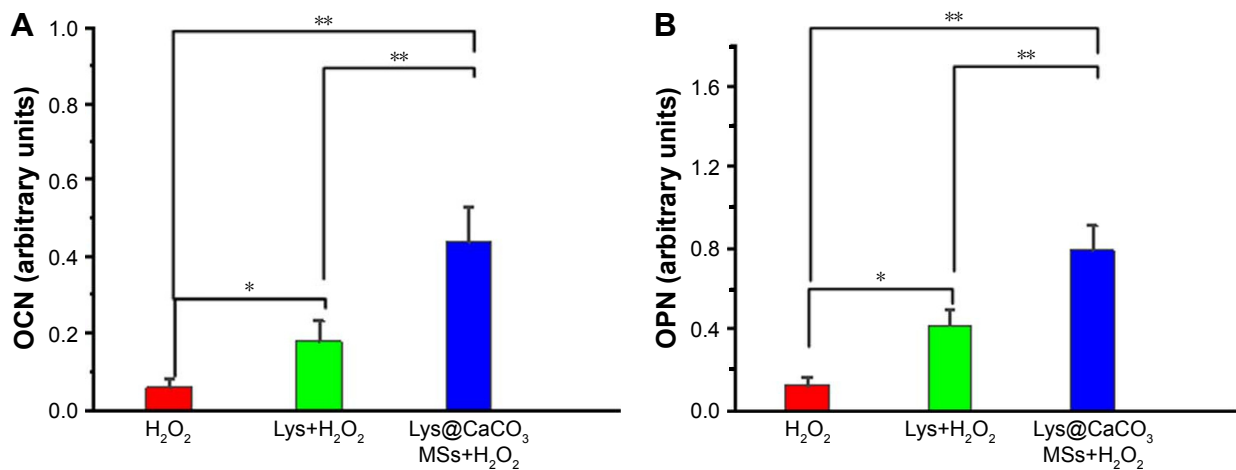**Abbreviations:** Lys, L-lysine; MSs, microspheres.

Figure S3 Quantification analysis results.
Notes: Quantification analysis results of the expression of OCN (**A**) and OPN (**B**) in H$_2$O$_2$-treated, Lys (0.8 mM)+H$_2$O$_2$-treated and Lys@CaCO$_3$ MSs (containing 0.8 mM Lys)+H$_2$O$_2$-treated groups, respectively (*$P<0.05$, **$P<0.01$, n = 3, each group treated with 80 μM H$_2$O$_2$ at pH = 5.5).
Abbreviations: Lys, L-lysine; MSs, microspheres; OCN, osteocalcin; OPN, osteopontin.
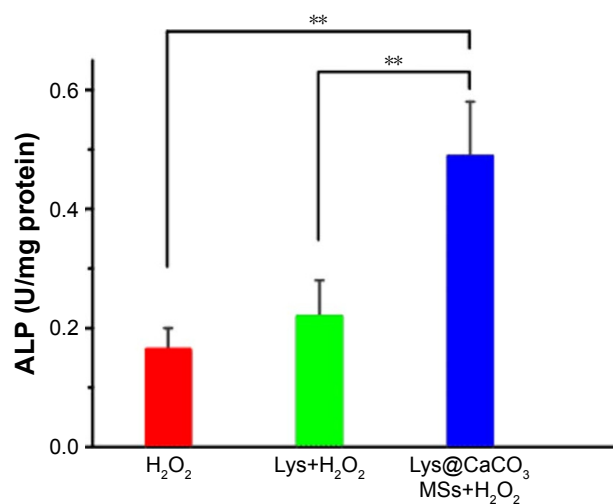
Figure S4 ALP activity analysis results of cells in H_2O_2-treated, Lys (0.8 mM)+H_2O_2-treated and Lys@CaCO$_3$ MSs (containing 0.8 mM Lys)+H_2O_2-treated groups, respectively (**P<0.01, n = 3, each group treated with 80 µM H_2O_2 at pH = 5.5).
Abbreviations: ALP, alkaline phosphatase; Lys, L-lysine; MSs, microspheres.